RSC Advances

PAPER

View Article Online
View Journal | View Issue

Cite this: *RSC Adv.*, 2023, **13**, 10110

Determination of active sites on the synthesis of novel Lewis acidic deep eutectic solvent catalysts and kinetic studies in microalgal biodiesel production†

Ange Douglas Potchamyou Ngatcha,[a] Anqi Zhao,[b] Shen Zhang,[ac] Wenlong Xiong,[ac] Moinuddin Sarker,[d] Jingliang Xu*[ac] and Md. Asraful Alam*[ac]

Experimental and theoretical considerations for kinetic modeling of the transesterification reaction of microalgae lipids into biodiesel were investigated using Lewis acid deep eutectic solvents (DESs) as a catalyst. The acid sites involved in the reaction were characterized using acetonitrile as a probe to understand the mechanism. DES ChCl–$SnCl_2$ (choline chloride–tin ii chloride) showed higher catalytic activity in transesterification due to its higher acidity compared to DES ChCl–$ZnCl_2$ (choline chloride–zinc chloride). This was illustrated by geometric optimization of the DES structures through density functional theory (DFT) which showed that the metal centers furthest from the choline moiety are the most acidic and the bond lengths of Sn–Cl were between 2.56 and 2.77 Å, and were greater than the Zn–Cl bond lengths from 2.30 to 2.48 Å, making the ChCl–$SnCl_2$ DES more acidic and more suitable for the biodiesel production. The fatty acid methyl ester (FAME) conversion from microalgae lipid was 36.75 mg g^{-1} under ideal conditions (6 molar ratio methanol–lipid with 8 vol% DES dosage in methanol at 140 °C for 420 min). The activation energy is found to be 36.3 kJ mol^{-1} based on the pseudo-first-order reaction, in addition, the DES catalyst (ChCl–$SnCl_2$) drove the reaction chemically and did not show mass transfer limitation. Information from this study can help to advance the development of an efficient and environmentally friendly industrial biodiesel production technology.

Received 25th January 2023
Accepted 22nd March 2023

DOI: 10.1039/d3ra00543g

rsc.li/rsc-advances

1. Introduction

The world's rapid population growth, along with rising industrialization and living standards, is the primary contributor to energy scarcity and global warming. Scientists are looking at the most viable alternative energy sources because of the ongoing depletion of fossil fuel reserves and rising environmental degradation and have obtained net zero emissions energy systems.[1,2] Renewable energy is cleaner and more efficient than traditional fossil fuels. Biomass energy is one of the most effective ways to replace traditional fossil fuels because it is widely available, renewable, and environmentally safe. Currently, there are a variety of uses for biomass in many industrial applications such as energy.[3,4]

Biomass-derived biodiesel has become increasingly popular because of the advantages it offers. Not only is biodiesel renewable, but it is also biodegradable, environmentally benign, and non-toxic; hence, it is a good substitute for diesel fuel.[5] The important characteristics of biodiesel are the same as those of diesel fuel produced from fossil fuel refineries and it also possesses high flash points, high cetane numbers, low viscosities, and high lubricity certifications.[6] In addition, biodiesel can satisfy global energy demand while achieving economic and environmental sustainability. Earlier studies have suggested that lignocellulose and microalgae could be better source for biodiesel production. Many microalgae strains reported having 15–300 times higher lipid content than the various common oil crops, thus proposing it as an alternative future source of biodiesel.[7]

FAME or biodiesel are produced by transesterification reaction of triacylglycerides (a noteworthy constituent of oils and fats) and esterification of free fatty acids using short-chain alcohol in the existence of a catalyst. The choice of catalyst has a significant impact on the production and selectivity of biodiesel as well as the transesterification process.[8] The process of transesterification, in which triacylglycerides are combined with alcohol in the presence of a homogeneous or

[a]School of Chemical Engineering, Zhengzhou University, Zhengzhou 450001, Henan, China. E-mail: xujl@zzu.edu.cn; alam@zzu.edu.cn; Fax: +86-371-67781801; Tel: +86-130-83608578

[b]School of Life Sciences, Zhengzhou University, Zhengzhou 450001, Henan, China

[c]State Key Laboratory of Motor Vehicle Biofuel Technology, Zhengzhou University, Zhengzhou 450001, Henan, China

[d]Waste Technologies LCC, Bridgeport, CT-06606, USA

† Electronic supplementary information (ESI) available. See DOI: https://doi.org/10.1039/d3ra00543g

heterogeneous catalyst and then subjected to heat, is the most commonly used method of producing biodiesel.[9] Currently, acids or their derivatives, such as toluene sulfonic acid and sulfuric acid (H_2SO_4)[10] are the traditionally applied catalysts for the transesterification of biodiesel, however, sulfuric acid suffers from serious drawbacks, such as equipment corrosion and pollution.[11] As a result, efforts should be devoted to develop green and efficient catalysts to solve the aforementioned challenges, such as equipment corrosion and environmental contamination, in the biodiesel production process.[12]

DESs are similar to ionic liquids (ILs) and well-integrated in the fields related to bioprocessing, extraction of compounds. DESs differ from ILs due to their impressive properties, such as easy process and relatively cheap synthesis design, and less volatile, biodegradable, and nontoxic solvent. Quaternary ammonium salts are cationic and typically used as hydrogen bond acceptors (HBA) in the synthesis of DES, whereas metal halides or organic compounds with hydrogen functional groups are used as hydrogen bond donor (HBD). DESs have been exploited in multiple aspects in the application fields of biodiesel production as co-solvent of biodiesel production.[13] Abbott effectively removed glycerol from biodiesel product blends by using DES salt–glycerol (1 : 1).[14]

The hydrogen functional bonding groups provide a mixture of Lewis or Brønsted acidic character, where various cation and/or anion molecules are present depending on their usage (HBD or HBA).[11] The application of DES with an acid character in the production of biodiesel has been reported by Tao *et al.*, where they used ChCl–$ZnCl_2$ for the production of biodiesel from the soybean oil but the yield has proved to be unsatisfactory,[15] it appears that the production of biodiesel is strongly influenced by the strength of the acid character of DES. According to our knowledge, studies on transesterification for biodiesel production from microalgae using DESs directly as catalysts and reaction media have not been reported before.

In this study, the catalytic activity of DESs synthesized was investigated in transesterification of microalgae lipid into biodiesel production. The DESs acid sites involved in the transesterification reaction were also investigated. (DFT) methods were used to optimize the DES structures in order to demonstrate that the acid strength of DESs is correlated to its catalytic activity. Optimization of biodiesel production was performed through several experimental factors in order to optimize the levels of reaction conditions including DES dosage in methanol, temperature, time and molar ratio methanol to lipid. A kinetic study is also described in order to understand their reaction mechanism. This work provides a technological alternative of environmentally safe catalyst for the process integration of biodiesel from microalgae.

2. Materials and methods

2.1. Materials

Chlorella pyrenoidosa microalgae was obtained from the Yunnan Baoshan Zeyuan Microalgae Health Technology Co. Ltd., China, and kept at 4 °C for experimental usage. A total of 20.31% of the maximum lipid content was recorded in this strain based on the conventional modified Floch's method.[16] Analytical grade chemicals used in experiments such as methanol, *n*-hexane, $SnCl_2$, $ZnCl_2$, methyl pentadecanoate (>98%), H_2SO_4 (~98%), and acetonitrile were purchased from Aladdin Industrial Corporation, Shanghai, China.

2.2. Preparation of the deep eutectic solvent catalyst

DESs ChCl–$ZnCl_2$ and ChCl–$SnCl_2$ were synthesized following the procedure reported by Cao *et al.*[17] at a ratio of 1 : 2. In that purpose, 0.1 mol of dried ChCl was mixed with 0.2 mol of $SnCl_2$, $ZnCl_2$ into the flask (250 mL) and heated in a water bath at 100 °C. Then, synthesized DESs were wrapped and kept in a desiccator to prevent it from absorbing moisture from the environment. The ratio of individual component during synthesis of ChCl–$ZnCl_2$ and ChCl–$SnCl_2$ DESs were selected based on a report by Liang *et al.*,[18] in which both DESs were applied as catalysts.

2.3. Characterization and confirmation of DESs

The DES formation was confirmed by performing Fourier-transform infrared (FT-IR) and proton nuclear magnetic resonance (^{1}H NMR). The instruments were an FTIR (BRUKERTENSOR II-USA) and an NMR (BRUKER AVANCE III 400 MHz) spectrometer. A thermogravimetric analysis (TGA) analyzer (NETZSCH, Germany) was used to analyse the thermal behaviour of DES. The targeted Lewis acid DES was characterized by FTIR measurement in a frequency ranging from 4000 to 500 cm^{-1}, and the acetonitrile has been used as a probe. In brief, the DES was mixed with acetonitrile under a ratio of 1 : 5 based on the procedure previously reported by ref. [19].

In order to gain more insights into the role of DESs in the production of biodiesel, quantum chemical methods were applied. (DFT) was used in that purpose as implemented in the Gaussian 09 suite of programs.[20] The B3LYP[21] hybrid functional[21,22] was combined to the Los Alamos double zeta (LanL2DZ) basis set[23] to perform the geometry optimizations without any constraint of symmetry. Frequency calculations performed on the relaxed structures of the DESs reveal no imaginary frequency, showing that all obtained structures are real minima of the potential energy surface. Mulliken's atomic charges were further determined in other to analyse the sites of LADESs prone to nucleophilic attacks.

2.4. Biodiesel production

The lipid was extracted using the optimum conditions reported in the previous study.[24] 200 mg of pre-treated microalgae and 6 mL methanol–*n*-butanol (1 : 4, v/v) were mixed in a 25 mL glass tube and magnetically stirred at temperature 60 °C controlled device (IKA C-MAG HS 7). After the reaction, the mixture was cooled at room temperature, 1.5 *n*-hexane and 3 mL distilled water were added to isolate lipids from the fraction *via* phase separation. A centrifuge (Beckman Coulter) was used at 10 min at 3500 g to separate the mixture from the liquid and solid phases. After the uppermost layer containing the lipids was put into a decanter that had been previously weighed for solvent

evaporation using a rotary evaporator (RE2000A, Shanghai, China).

The procedures described by Lu *et al.*[25] were used to methylate the isolated lipid to obtain the FAME. In brief, 0.019 g of lipids extracted under optimized conditions were placed into each glass tube and transesterified based on the experiment design parameters including DES dosage in methanol (1 to 9% v/v, temperature (from 100 to 160 °C), time (60 to 540 min), and molar ratio of methanol to lipid (3 to 12 v/w). Then, the mixture was allowed to cool at room temperature for 20 min. Subsequently, the 5 mL of *n*-hexane was added in the mixture and centrifuged for 5 min at 3500*g* to create a binary phase for separating FAME. Afterward, the uppermost layer of hexane containing FAME was transferred to a different gas chromatography (GC) sample ampoule for further analysis. The results of the qualitative analysis of FAMEs were obtained using a GC (Agilent, USA 8890) following the setting of previous studies.[24,26]

Then, the total weight of FAME was estimated based on the procedure reported in the literature[27] using the following equation:

$$W_{FA} = A_S/A_{IS} \times C_{IS}/W_S \quad (1)$$

A_S represents the peak area of the fatty acid in the sample in GC-mass chromatogram, whereas A_{IS} is the peak area of internal standard in GC-mass chromatogram. C_{IS} stands for the concentration of internal standard (mg). W_S and W_{FA} are the weights of the biomass sample (g) and the FAME (mg g^{-1}) respectively.

The amount of lipid exterifiable into FAME was calculated using a conventional modified Folch's method and compared with the traditional H_2SO_4 catalyst-based data.[24]

2.5. Kinetics of transesterification reaction

Herein, the effects of temperature and time on the reaction were examined to better understand the reaction's kinetics. A transesterification reaction at different temperatures ranging from 100 to 140 °C was performed to find the activation energy. The activation energy and rate constant of a pseudo-first-order reaction were calculated using eqn (2) and (3).

$$-\ln(1 - X_{FAME}) = kt \quad (2)$$

$$\ln k = \ln A - E_a/RT \quad (3)$$

where X is the FAME conversion from microalgae lipid at time t and k is the rate constant of the pseudo-first-order reaction in minutes. In these equations, A stand for frequency factor, R indicated the universal gas constant and T denote absolute temperature. The calculated slope and intercept will reveal the values of the activation energy and frequency factor if $\ln k$ is plotted against $1/T$.

3. Results and discussions

3.1. Confirmation of deep eutectic solvent formation and characterization

3.1.1. FT-IR spectra of the formation of DESs synthesized. The infrared spectra of ChCl–$SnCl_2$ and ChCl–$ZnCl_2$ are shown in Fig. 1a and b. For ChCl–$SnCl_2$ (Fig. 1a), the FTIR spectrum of ChCl showed the representative bands allied with OH, CH_2, CH_3, and C–N^+ groups at 3250 cm^{-1} (O–H stretch), 1465–1432 cm^{-1} (CH_3 and CH_2 bend), 1036 cm^{-1} (C–O stretch), and 862 cm^{-1} (C–N^+ symmetric stretching). Hence, numerous bands conforming to choline chloride co-exist after DES formation, the band between 3100 and 3490 cm^{-1} can be assigned of stretching vibrations of the OH bond of $SnCl_2$ in DES and O–H stretching is responsible for the vibrational band at 3490 cm^{-1}. A widening is observed in this band caused by water molecules, thereby indicating the establishment of hydrogen bonds. The H–O–H bending vibration appears in the region between 1609 and 1623 cm^{-1}, Sn–Cl and Sn–OH bonds have absorption bands below 925 cm^{-1} and the absorption corresponding to C–N^+ symmetric stretching is observed at 866 cm^{-1}. The identical similarity is also observed with other studies that have synthesized the same DES.[28]

Meanwhile, the FTIR ChCl–$ZnCl_2$ was represented in Fig. 1b, the ChCl characteristics are almost identical to those of the previous DES ChCl–$SnCl_2$ synthesized. However, 1070 and 966 cm^{-1} bands could be interpreted as symbolizing the anti-symmetric C–O and C–C–O stretching vibrations associated with the NC_2H_4OH group of the choline cation. The ChCl–$ZnCl_2$

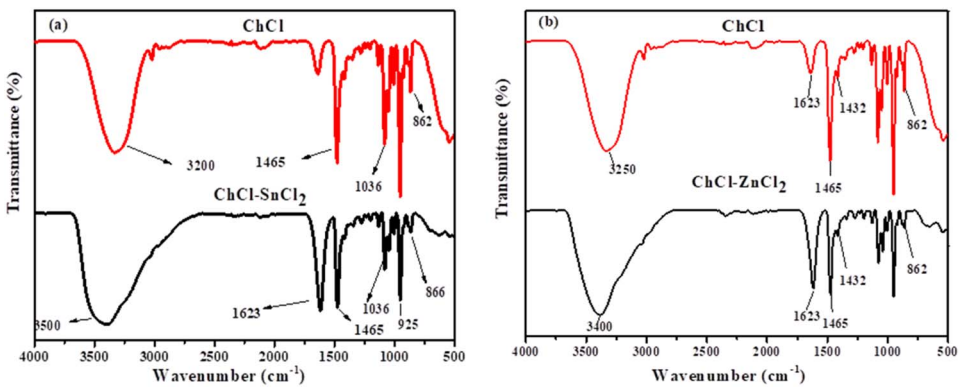

Fig. 1 FTIR spectra of different DESs (a) ChCl–$SnCl_2$ and (b) ChCl–$ZnCl_2$ at (1 : 2) molar ratio.

showed the peak at 1094 and 986 cm^{-1} being materialized. The characteristic peaks for CN anti-symmetric stretching vibration were easily detected in the relatively lower bands (1029–1146 cm^{-1}). The –OH portion might be attributed to the bands between 3250 and 3487 cm^{-1}. The confirmation of this DES is consistent with the report made by Fanglong *et al.*[29]

3.1.2. ^{1}H NMR spectra of ChCl–$ZnCl_2$, ChCl–$SnCl_2$. A direct 5 mm broadband probe was used to perform ^{1}H NMR measurements at 400 MHz. The solvent utilized was dimethyl sulfoxide (DMSO), and the temperature was set at 298 K. In addition, the chemical shifts or changes were accredited to tetramethylsilane (TMS) as an external reference and were presented as δ ppm values based on TMS. Moreover, proton coupling patterns were defined as singlet (s), doublet (d), doublet of doublets (dd), triplet (t), triplet of doublets (td), multiplet (m), and quartet (q).

^{1}H NMR (400 MHz, DMSO) δ 5.28 (t, $J = 4.6$ Hz, 1H), 3.83 (s, 2H), 3.39 (d, $J = 5.1$ Hz, 2H), 3.10 (s, 9H) were recorded from the experimental spectrum data of ChCl–$ZnCl_2$ and presented in Fig. 2a. The ^{1}H NMR data permits the identification of several atoms or molecules present in the of ChCl–$ZnCl_2$ DES showed various essential structural traits (as shown in Fig. 2a) including the signals of the hydroxyl hydrogen in choline ($\delta = 5.28$ (t, 1H, and H_d)). Strong signals at 3.10 (s, 9H, and H_a) correspond to the protons of methyl groups connected to nitrogen in choline. ChCl contains two methylene groups, one of which is connected to nitrogen and the other to hydroxyl. The signal of 3.83 ppm (s, 2H, and H_b) is assimilated to the protons of the methylene group coupled to nitrogen while as the signal of 3.39 ppm (d, 2H, H_c) corresponds the protons of the methylene group attached to hydroxyl.

^{1}H NMR (400 MHz, DMSO) δ 5.31 (t, $J = 4.9$ Hz, and 1H), 3.83 (dd, $J = 6.1$, 3.8 Hz, and 2H), 3.40 (d, $J = 5.2$ Hz, and 2H), 3.11 (s, 9H) were obtained from the experimental spectrum data of ChCl–$SnCl_2$ and presented in Fig. 2b. We can distinguish the various atoms in the ChCl–$SnCl_2$ mixture using the ^{1}H NMR spectrum. This mixture displayed numerous significant structural features, such as the signals of the hydroxyl hydrogen of the choline (($\delta = 5.31$ (t, 1H, and H_d)). The strong signals at 3.11 (s, 9H, H_a) represent the protons of the methyl groups linked to the nitrogen of the choline. Moreover, ChCl has two methylene groups, one of which is covalently bonded to nitrogen and the

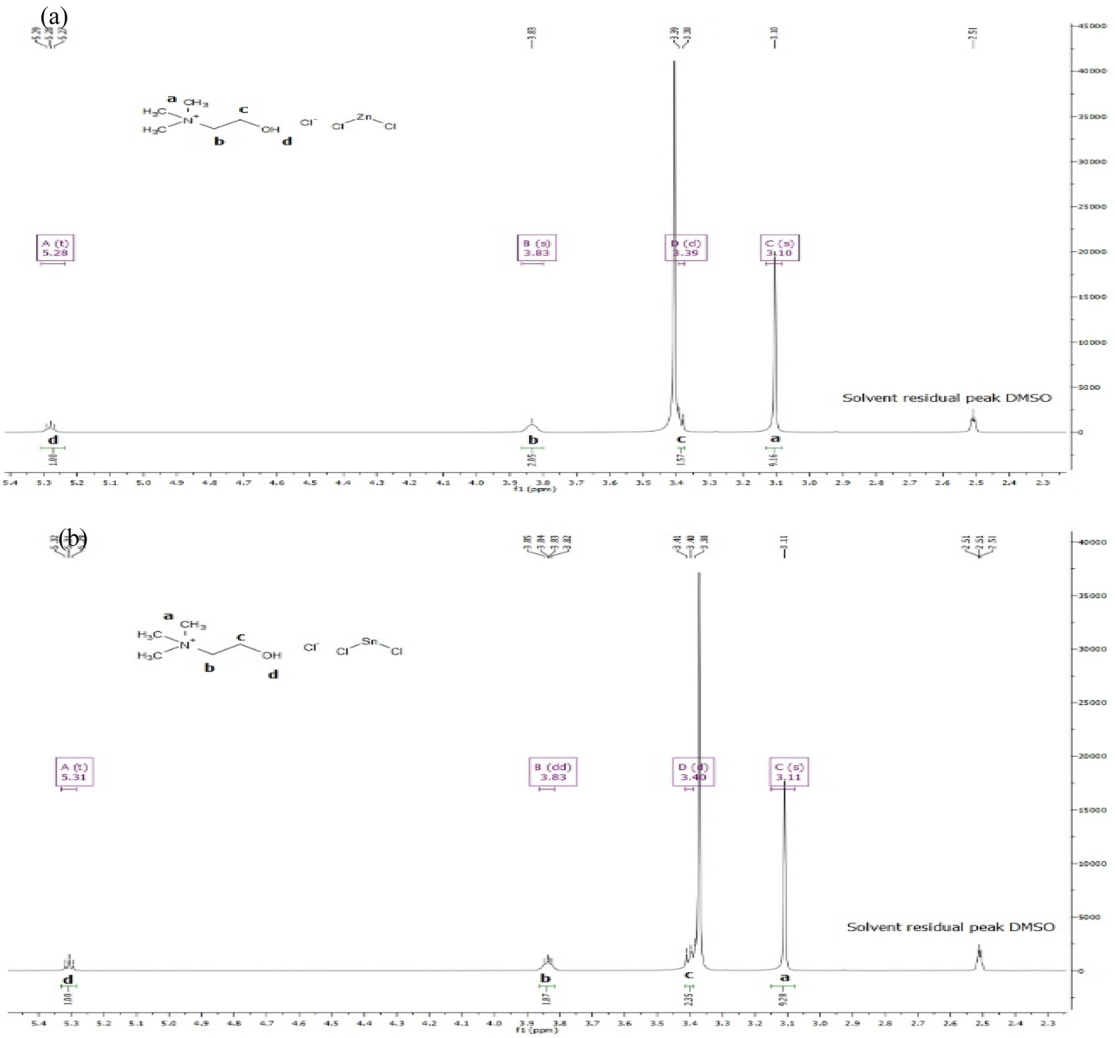

Fig. 2 ^{1}H NMR of DES (a) of ChCl–$ZnCl_2$ and (b) ChCl–$SnCl_2$ at (1 : 2) molar ratio.

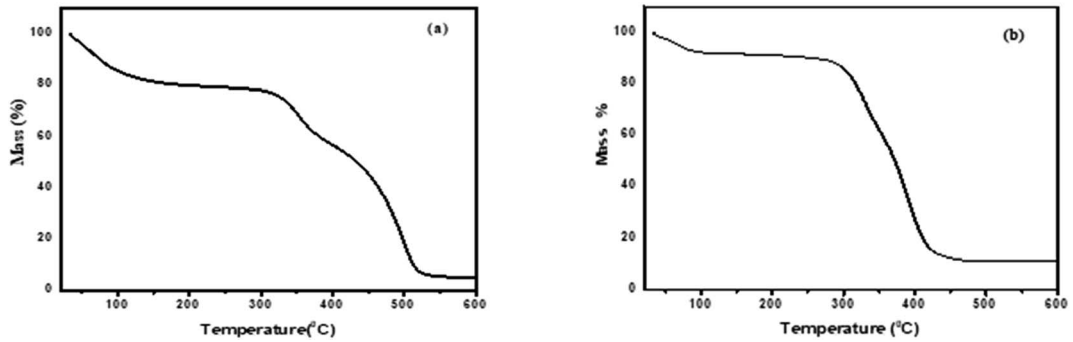

Fig. 3 Thermogravimetry curves of DESs (a) ChCl–$ZnCl_2$ and (b) ChCl–$SnCl_2$ at (1 : 2) molar ratio.

other is covalently bonded to hydroxyl. The signal at 3.83 ppm (dd, 2H, and H_b) represents the protons of the methylene group bound to the nitrogen, whereas the signal at 3.20 ppm (d, 2H, H_c) correlates to the protons of the methylene group that are linked to the hydroxyl.

3.1.3. Thermogravimetric analysis. Fig. 3 illustrates the thermogravimetric (TG) analysis. ChCl–$ZnCl_2$, and ChCl–$SnCl_2$ have a decomposition temperature of 321.81 °C and 300.41 °C, respectively. However, a mass loss is observed near 100 °C from water evaporation on the TG curve. Consequently, ChCl displays high thermal stabilities in present study which is consistent with earlier study.[15]

3.1.4. Determination of Lewis acid sites. Acetonitrile is a Lewis base that has only been reported to determine Lewis's acidity. Thus, we used the acetonitrile the like probe to determine the Lewis acidity sites from our DESs. The band between 2250 and 2300 cm^{-1} appears from all DES mixtures with acetonitrile, hence, a mixture containing acetonitrile and Lewis acid material could give rise to a new distinctive peak at 2250–2350 cm^{-1} (Fig. 4a and b), which arises from the complex compound (CN–Lewis complex) of Lewis acid material and acetonitrile.[12,30]

3.1.5. Geometry optimization of the DESs structures. The optimized structures of these DES are depicted in Fig. 5 and 6. Analysis of these figures reveals that the Zn–Cl bond length in ChCl–$ZnCl_2$ (1 : 2) ranges 2.30–2.48 Å, whereas the Sn–Cl bond length ranges 2.56–2.77 Å. The high value of the Sn–Cl bond length is because Sn has a greater atomic radius than Zn. These values support the dative nature of the previously mentioned bonds. Fig. 5 and 6 also show graphical representations of the atoms' Mulliken atomic charges. Herein, the atoms with positive charges (electron poor sites) and negative charges (electron-rich sites) are represented by green and red colors, respectively, whereas neutral sites (with a charge close to zero) are represented by black, as shown in Fig. 5 and 6. Hence, it is evident from these figures that the metallic centers have positive charges, which are the highest values of Mulliken charges in all complexes, thereby indicating they are Lewis's acid sites. The charges of Zn and Sn atoms are 0.567–0.668, and 0.878–0.883*e*. In each of these structures, the metal centers farther from the choline moiety are the most acidic.

3.1.6. Characterization of extracted lipid. FTIR was used to determine the lipids extracted by our previous method for compliance with the adaptation of these lipids for the synthesis of FAME (biodiesel). The following characteristic peaks of the lipids are represented in Fig. 7. Thus, 3005 cm^{-1} denotes the = C–H stretch in the fatty acids of TAGs. Meanwhile, stretching CH_3 of acyl chains in fatty acids of TAGs is represented by 2955 cm^{-1} and 1375 cm^{-1}; stretching CH_2 of acyl chains in fatty acids of TAGs is represented by 2925 cm^{-1}, 2850 cm^{-1}, and 745 cm^{-1}; and the peak, 1666–1746 cm^{-1}, represents amide I band (C=O stretching), N–H bending (amide II). However, the

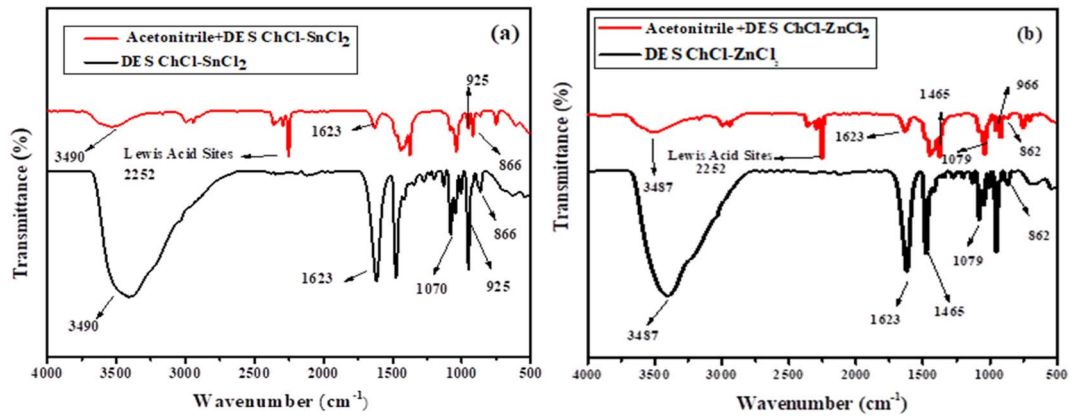

Fig. 4 FTIR spectra of the DESs prepared with acetonitrile using as probe. (a) Acetonitrile + ChCl–$SnCl_2$ and (b) acetonitrile + ChCl–$ZnCl_2$.

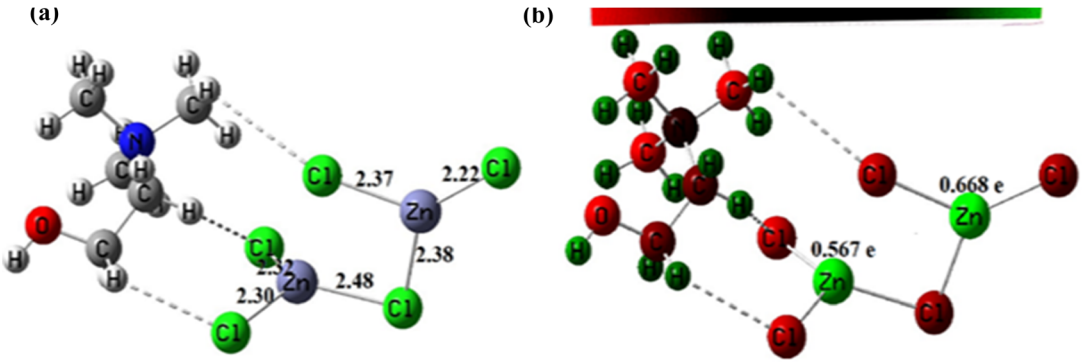

Fig. 5 (a) Optimized structure of ChCl–$ZnCl_2$ (1 : 2) and (b) Mulliken's atomic charges of its atoms obtained at DFT/B3LYP/Lan12DZ level of theory.

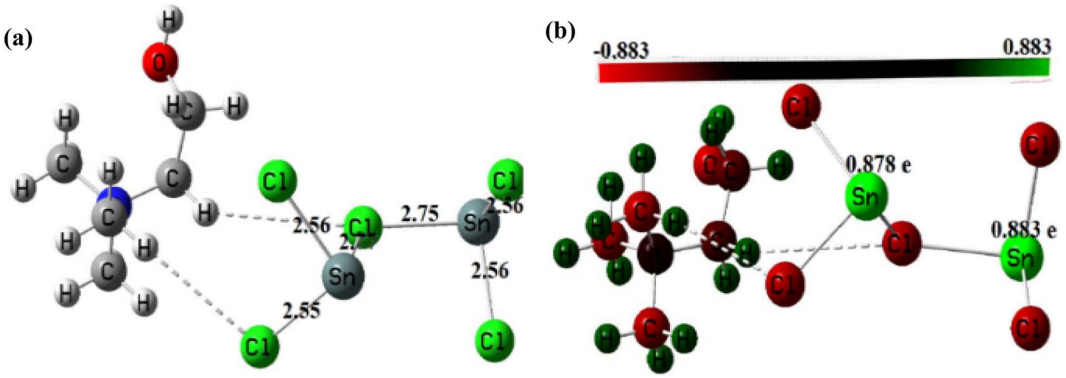

Fig. 6 (a) Optimized structure of ChCl–$SnCl_2$ (1 : 2) and (b) Mulliken's atomic charges of its atoms obtained at DFT/B3LYP/Lan12DZ level of theory.

peaks of 1746 cm^{-1} representing C=O stretching in ethyl esters are relatively very low. This may specify that the share of free fatty acids (FFA) is low as compared to the share of triacylglycerols (TAG) in the extracted lipids by previous methods.[31,32]

3.2. Screening of the catalyst

In this study, the catalytic activity of different DES synthesized for biodiesel production was investigated using two-step biodiesel production approach. In brief, DES ChCl–$SnCl_2$ and ChCl–$ZnCl_2$ were tested based on the same conditions of the following parameters: molar ratio methanol to lipid 6, the temperature at 100 °C, time 180 min, and DES dosage in methanol 5 vol%. Fig. 8 shows that the FAME weight of DES ChCl–$SnCl_2$ is 7.80 mg g^{-1}, which is higher than the FAME weight of DES ChCl–$ZnCl_2$, which is 1.80 mg g^{-1}. All DES have the same HBA ChCl, indicating that it was the HBD differences of the Lewis acids ($SnCl_2$, $ZnCl_2$) that enhanced the catalytic performance in the reaction. It has been reported in previous studies that acid strength greatly influences the yield of biodiesel production.[15] It is possible that the high catalytic

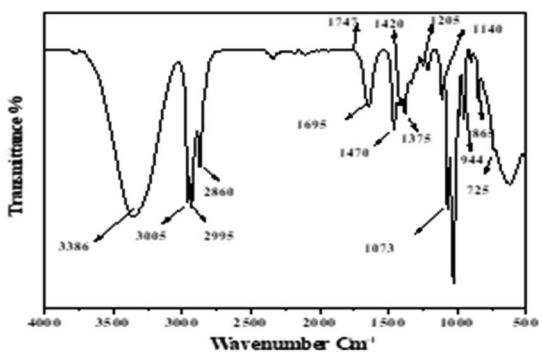

Fig. 7 Biochemical profiles of the lipids extract by methanol/*n*-butanol presenting functional groups.

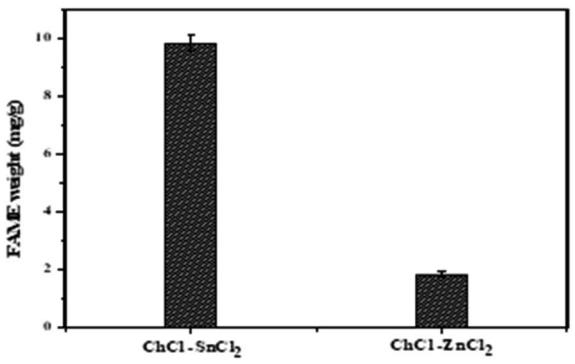

Fig. 8 Catalyst DESs screening performance for transesterification of lipid into FAME.

Table 1 Biochemical profile of the lipids extract by methanol/*n*-butanol presenting functional groups

Band (cm^{-1})	Peak identification	Molecules
3005	C–C unsaturated fatty acids	Lipid
2931	CH_2 asymmetric stretching	Lipid
2869	CH_2 symmetric stretching saturated fatty acid	Lipid
1666–1736	Amide I band (C=O stretching), N–H bending (amide II) Ester C–O stretching	Lipid, protein
1470	CH_2 deformation	Lipid
1375	N–H bending (amide II)	Lipid
1140	C–O–C stretching	
1073	P–O stretching (symmetric) of $>PO_2$	Polyphosphate, phospholipid
900–1200	C–O and C–C stretching, C–O–H and C–O–C deformation	Polyphosphate, phospholipid
865	P–O–P stretching	Polyphosphate, phospholipid
745	CH_2 deformations	Lipid

Table 2 Fatty acid methyl ester profile

Fatty acids	Designation compound	FAME weight (mg g^{-1})	Total weight (mg g^{-1})
Saturated fatty acid (SFA)			
Hexadecanoic acid	C16:0	8.87 ± 0	8.87
Monounsaturated fatty acids (MUFA)			
Methyl palmitoleate	C16:1	0.85 ± 0.45	1.16
Methyl oleates	C18:1	0.31 ± 0.32	
Polyunsaturated fatty acids (PUFA)			
Hexadecadienoic acid	C16:2	4.21 ± 0.30	26.56
7,10,13-Hexadecatrienoic acid	C16:3	4.76 ± 0.17	
9,12-Octadecadienoic acid	C18:2	11.36 ± 0.78	
9,12,15-Octadecadienoic acid	C18:3	6.23 ± 0.74	

performance of DES ChCl–$SnCl_2$ is due to its higher acidity than DES ChCl–$ZnCl_2$. This is demonstrated by geometric optimization of DES structures (Fig. 5 and 6), which revealed that metal centers farthest from the choline moiety are the most acidic, and the DES ChCl–$SnCl_2$ shows metal centers farther from the choline moiety, the bond lengths of Sn–Cl were between 2.56 and 2.77 Å which was greater than the Zn bond lengths –Cl from 2.30 to 2.48 Å, making DES ChCl–$SnCl_2$ more acid and more suitable for biodiesel production (Tables 1 and 2).

A carbocation is created when the carbonyl oxygen of carboxylic acid from triglyceride interacts with the acid sites of DES. Alcohol's nucleophilic attack on the carbocation forms a tetrahedral intermediate and eliminates HOH to create a diglyceride and methyl ester (Fig. 9). In order to confirm the catalytic ability of the DES used herein, the first step of the above-mentioned mechanism was simulated at DFT/B3LYP/Lanl2DZ level of theory, by replacing the initial triglyceride by acetic acid to reduce the size of the molecular system to compute. The adsorption reaction (of acetic acid on the DES) was simulated herein through a Lewis type acid–base reaction between the carbonyl O-atom (base) of acetic acid and the metal center of each catalyst farther from the choline moiety, previously identified as the most acid sites. This led to dative M–O (M = Sn and Zn) bonds between these atoms. The negative values of the calculated Gibbs free energy of adsorption (ΔG) interestingly show that the reaction is spontaneous in standard conditions with all catalysts. The reaction with ChCl–$SnCl_2$ is the most the spontaneous ($\Delta G = -18.59$ kcal mol^{-1}), surely due the high acidy of the Sn ion as compared to Zn ions ($\Delta G = -10.88$ kcal mol^{-1}). This high acidy leads to stronger interactions between the acetic acid and the Sn ions. The Zn–O and Sn–O bond distances after adsorption are respectively 2.04 and 2.19 Å. Upon adsorption, the activation increases the charge of the carboxylic C-atom, making it more electropositive, and thus facilitate the nucleophilic attack by methanol. The Mulliken atomic charge of that C-atom is found to increase from 0.278 to 0.375 as well as 0.470*e* in presence of the, Zn and Sn metal ions respectively. Accordingly, the tin-based catalyst better activate this C-atom than the zinc based one and thereby corroborates the best acidity previously mentioned for the former. Therefore, we selected the DES ChCl–$SnCl_2$ for the next step of the experiment.

3.3. Optimization of the FAME extraction and analysis of the FAME profile

3.3.1. Effect of DES catalyst dosage in methanol. Herein, tests to investigate the DES dosage were carried out, with the DES dosage varying from 1 to 9 vol% under the conditions of temperature (100 °C), time (240 min), and molar ratio methanol

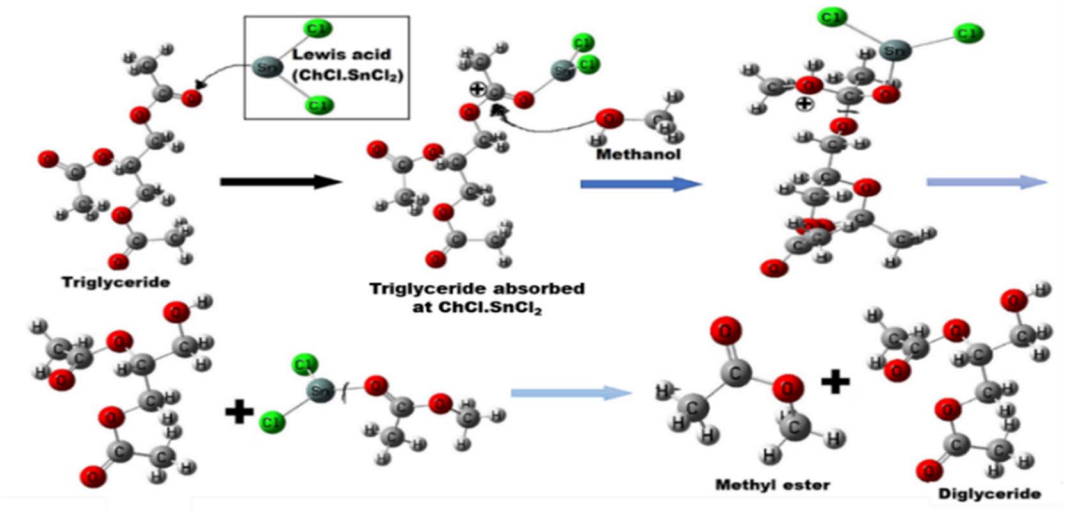

Fig. 9 Illustration of the mechanism of Lewis acid DES catalysed transesterification.

to lipid (6), as shown in Fig. 10a. Based on the results, the FAME weight increased from 4.41 mg g^{-1} to 15.88 mg g^{-1}. The hypothesis stated that the increase in the dosage of DES catalyst brings more acid catalytic sites to the direct transesterification reaction system, which then contributes to directly accelerate the reaction rate, the similar phenomenon was also reported in a study by Liu *et al.*[11] However, a little declination is observed when the DES dosage reaches 9 vol%. This could be explained by the fact that a high dosage rate of acid can negatively influence the transesterification process. Moreover, a higher concentration of catalyst over optimized level could cause the formation of an emulsion, favoring high viscosity of the carrier and hampering the recovery process of biodiesel. However, the reactants are more difficult to diffuse when the catalyst

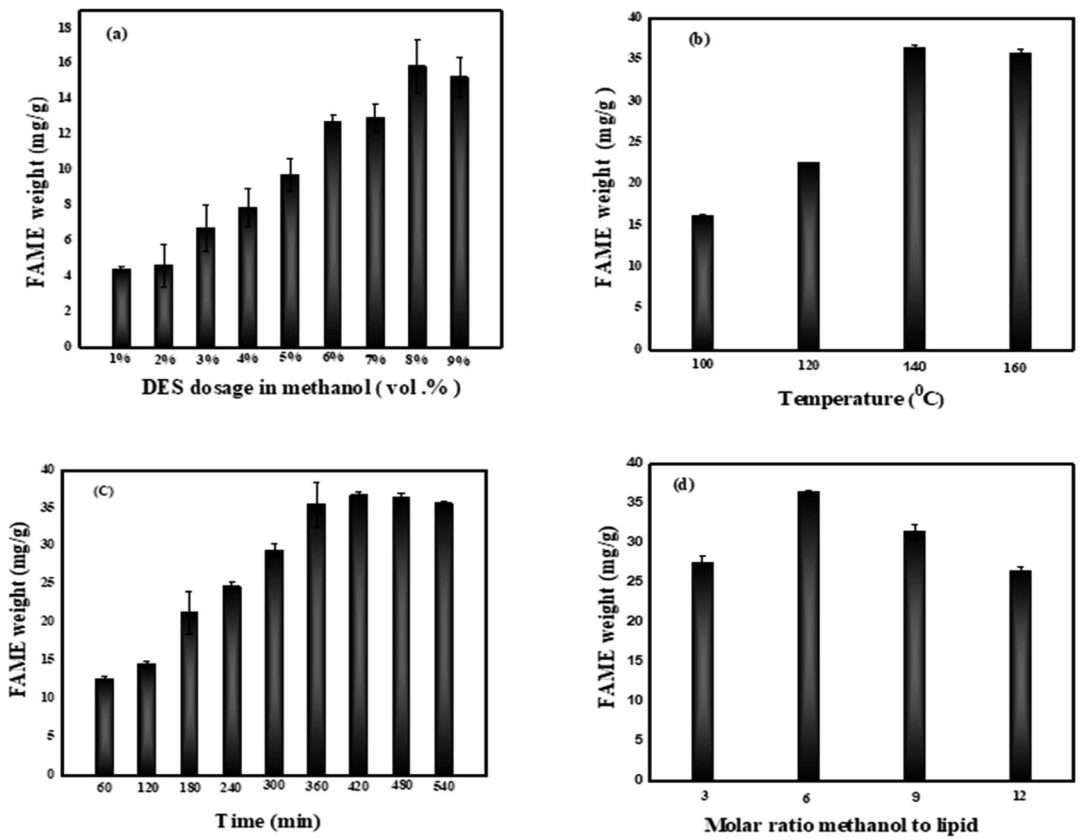

Fig. 10 Influence of different parameters for FAME extraction (a) DES dosage in methanol, (b) temperature, (c) time, and (d) molar ratio methanol to lipid.

concentration is too high. Higher diffusion resistance decreases the likelihood of reactants colliding, which can adversely affect the conversion efficiency.[33,34] Muhammad *et al.* and other studies reported a FAME yield increasing proportionally with acid catalyst dosage, but a slight depletion was also recorded at a concentration of 4000 mL per kg dry biomass.[35] Meanwhile, in another study, Duongbia *et al.* showed this to have an advantage as to yield the best fatty acid; fatty acid production increased with the concentration rate of acid (1 M for 44.35%, over 3 M for 55.25%, and 4.5 M for 53.53% of fatty acid produced).[36] Considering the experimental results, 8 vol% DES dosage in methanol was adopted in the current experiment.

3.3.2. Effect temperature. According to most studies, the primary parameters that can influence kinetic modeling are time and temperature.[37] Hence, we investigated different temperatures ranging from 100 °C to 160 °C under the conditions of DES dosage of 8 vol%, time of 240 min, and molar ratio methanol to lipid of 6. The results shown in Fig. 10b indicated that when temperature climbed from 100 °C to 140 °C, FAME weight increased by 16.10 mg g^{-1} to 36.39 mg g^{-1}, reaching a maximum at 140 °C. A connection could be made between this experiment and extensive studies on the theory. The Arrhenius equation indicated that rising the reaction temperature could accelerate the reaction collision to increase the reaction speed.[11] Moreover, a modest reduction in FAME conversion efficiency was observed as the temperature rose above 140 °C probably due to the increase in the vapor pressure of methanol which is unfavorable for an exothermic reaction, resulting to a decomposition catalytic activity and a drop in the weight of FAME.[38] In addition, the viscosity of the oil decreases at high temperatures, which may justify the slight decrease observed at the temperature of 160 °C.[39] The results presented at this state guided the choice of the temperature of 140 °C as optimal temperature.

3.3.3. Effect of time. We have investigated different time values between 60 and 540 min under the DES dosage in methanol of 8 vol%, the temperature of 140 °C, and molar ratio of methanol to lipid of 6. Fig. 10c shows an increase in FAME weight as reaction time increases, reaching approximately 36.71 mg g^{-1} after 420 min indicating the high rate of the transesterification which can be explained a fairly high transesterification of glycerides due to the rate of forward reaction is significantly higher than the rate of reverse reaction. The relationship between FAME weight and time was found to be positively proportional. This statement is in agreement with other previous studies.[35,40] However, a slight decrease is observed between 480 and 540 min. These results imply that very high reaction times are not required to increase FAME yield because of factors such as solvent loss, overheating, energy expenditure, and FAME loss.[41] The reaction time at 420 min was adopted in the current experiment for next step.

3.3.4. Effect molar ratio of methanol to lipid. Experiments were carried out to determine the influence of the molar ratio of methanol to lipid on FAME weight with standardized temperature, time, and DES dosage in methanol set at 140 °C, 420 min and 8 vol% respectively to each parameter. The results showed in Fig. 10d indicates that, FAME weight increased significantly as the molar ratio methanol to lipid increased from 3 to 6, with a maximum of 36.75 mg g^{-1} achieved at a molar ratio methanol to lipid 6. The hypothesis evoked is that transesterification requires three moles of alcohol and one mole of triglyceride (TG) to make three moles of fatty acid alkyl ester and one mole of glycerol stoichiometrically. Too much methanol is the key thing that moves the equilibrium toward progress and makes FAME conversion better.[37] Another study found that increasing the volume of methanol from 1 to 4 mL raised the biodiesel production from 59.2 to 83.9%, with maximum biodiesel yields of 86.6% at 6 mL methanol.[37,42] A further rise in the molar ratio methanol to lipid caused a decrease in FAME weight. This could be related to the excessive dilution of the catalyst by methanol[43] which caused an undesirable reverse reaction appear. Same phenomenon was also observed in a recent study reported by Ying *et al.* (2020).[11] Furthermore, excess methanol dissolves glycerol. Hence, this process slows the rate of reaction and causes the equilibrium to move in the other direction.[43]

3.3.5. FAME profile at optimum condition. Fatty acids C16:0, C18:2, and C18:3 make up most of the volume, thereby accounting for 9.84, 12.48, and 5.95 mg g^{-1}, respectively. There were 26.56, 1.16, and 8.87 mg g^{-1} of polyunsaturated fatty acids, monounsaturated fatty acids, and saturated fatty acids, respectively, based on the qualitative examination of the fatty acids. The fatty acids C16–C18 have certain benefits for engine start-up, including low viscosity, and high oxidative consistency.[44] These fatty acids are the best candidates for biodiesel generation, C16:0, C18:0, C18:1, C18:2, and C18:3 are the most prevalent fatty acids present in plant biodiesel (canola, soybean, and palm).[45] A study reported the profile of fatty acids from strain *C. pyrenoidosa* is constituted of C16:0, C16:1, C18:1, C18:2, and C18:3.[46] Meanwhile, both saturated and unsaturated fatty acids were identified in our study. A similar fatty acid profile has been detected in *Chlorella* sp. and *Scenedesmus* sp. in previous study which is consistent with the present study.[47] Moreover, the methyl esters having C16 and C18 carbon chains have been identified as desirable for the production of higher-quality biodiesel in earlier study.[48]

3.3.6. Reaction kinetics. As indicated by eqn (4)–(6), three successive reversible reactions drive the transesterification of TG with methanol when the catalysts are available.

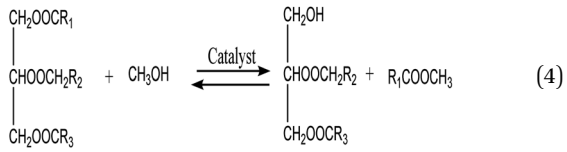

(4)

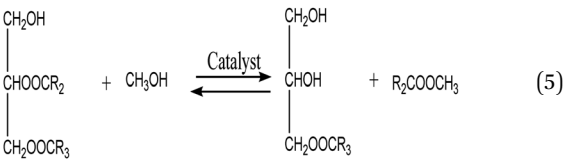

(5)

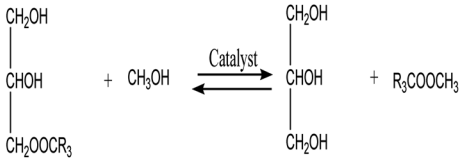

(6)

However, the transesterification of glycerides can be completed extensively given that the rate of forward reaction is significantly greater than the rate which reverse reaction occurred. As a consequence of this, the process of the aforementioned reaction can be simplified down to the one-step irreversible reaction that is outlined in eqn (7).

It is predicated on several hypotheses, including (a) that kinetics controls the rate of transesterification, (b) that intermediate products can be ignored; (c) that the reaction system is an ideal one; and (d) that reverse reaction is neglected.[43,49]

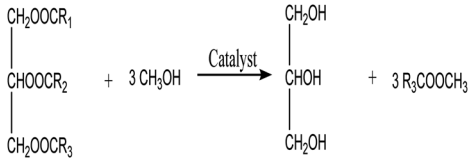

(7)

The formula for reaction rate can be written as follows using eqn (7):

$$-r_a = -\frac{d[TG]}{dt} = k'[TG][methanol]^3 \quad (8)$$

$$[TG] = [TG]_0(1 - X_{FAME}) \quad (9)$$

where r_a represents the reaction rate and k' represents constant of reaction rate, whereas, the concentrations of reactants are [TG] and [methanol]. [TG_0] denotes the starting concentration of TG, and X_{FAME} represents the FAME weight at t minute. In addition, [methanol] can be thought of as constant because the molar amount of methanol is substantially higher than that of the TG.

Consequently, the forward reaction can be thought of as a pseudo-first-order reaction, and the equations above are then changed to eqn (10) and (11).

$$-\frac{d[TG]}{dt} = k[TG] \quad (10)$$

$$\frac{dX_{FAME}}{dt} = k(1 - X_{FAME}) \quad (11)$$

where k is the adjusted reaction rate constant. Eqn (8) was created by integrating eqn (11). Meanwhile, it was discovered from eqn (12) showed a linear association between $-\ln(1 - X_{FAME})$.

$$-\ln(1 - X_{FAME}) = kt \quad (12)$$

and t. Fig. 11 depicts the temperature-dependent value of the reaction rate constant. The outcome of graphing $-\ln(1 - X_{FAME})$ against t based on the experimental data is clearly shown in Fig. 11(a–c). The straight line's slope indicates the reaction rate constant, that is k. The figures demonstrate that the earliest

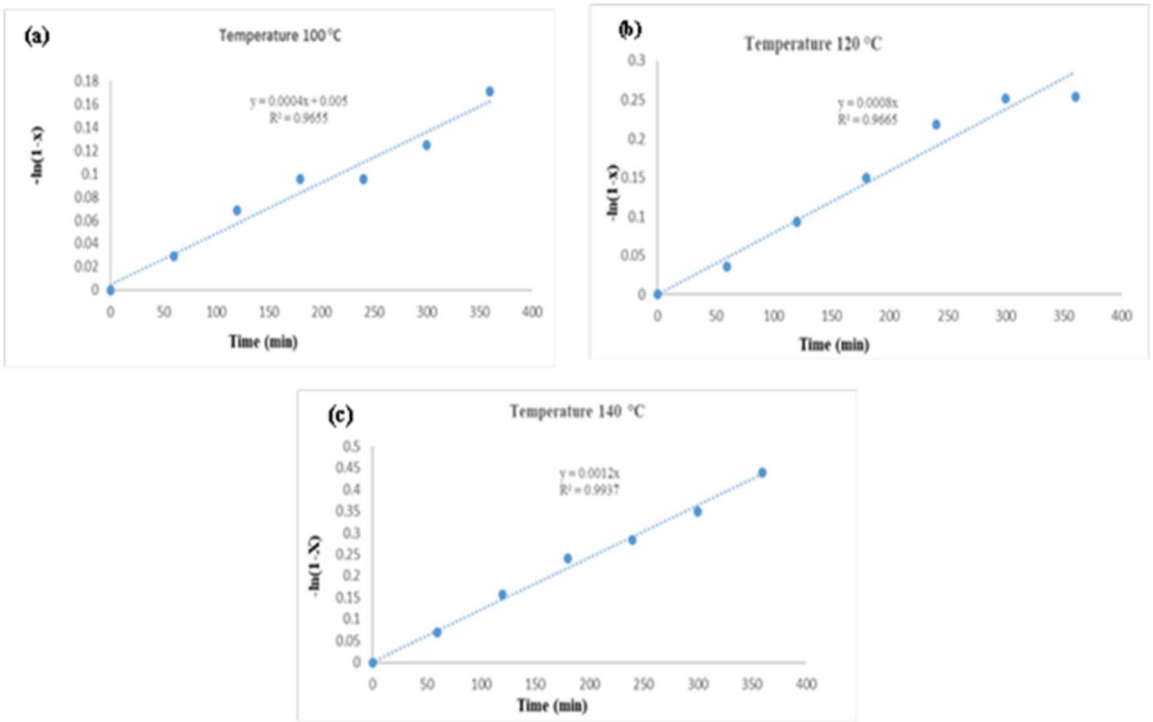

Fig. 11 Plots of $-\ln(1 - X)$ *versus* time for transesterification of microalgae lipid by DES ChCl–$SnCl_2$ (1 : 2) at divers reaction temperatures (a) 100 °C, (b) 120 °C, and (c) 140 °C.

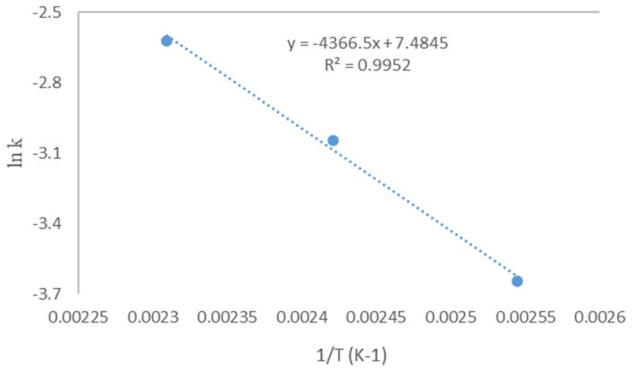

Fig. 12 Arrhenius plot between *K versus* 1/*T* for transesterification of microalgae lipid by DES ChCh–$SnCl_2$.

instances of the transesterification process have a sluggish reaction rate, but this rate after increases dramatically. Data analysis revealed that a 20 °C temperature doubles the constant rate.

A linear relationship was found by plotting $\ln(1 - X_{\mathrm{FAME}})$ *versus t*, thus confirming the theory that the conducted reaction is pseudo-first order. The slope of the regression equation connected to Fig. 11(a–c) was identified as the constant reaction rate at each temperature.

As evidenced, as predicted by the Arrhenius equation, the reaction rate constant rose as the temperature increased.

$$k = A_0 e^{-\frac{E_a}{RT}} \quad (13)$$

where E_a and A_0 represent the activation energy and pre-exponential factor, respectively. Eqn (13) can be changed as follows:

$$\ln k = \ln A_0 - \frac{E_a}{RT} \quad (14)$$

where E_a was determined to be 36.3 kJ mol^{-1}, and in some reports like Freedman *et al.*, the activation energy for heterogeneous catalysts ranged from 26 to 84 kJ mol^{-1}. Kaur and Ali observed 40.8 kJ mol^{-1} activation energy in the transesterification of cotton seed oil using a Li/ZrO_2 catalyst.[50] Lukić *et al.* discovered a 26.5 kJ mol^{-1} activation energy for soyabean oil using a CaO·ZnO catalyst.[51] A_0 was found at 1780.23383031 min^{-1} when ln *k* was plotted against 1/*T* as in Fig. 12. It is well-known from the literature that an energy activation in the range of 10–15 kJ mol^{-1} reveals a reaction rate controlled by mass transfer;[52] when the activation energy is greater than 25 kJ mol^{-1}, the reaction is chemically conducted. In this study, DES was used, and the activation energy was found to be 36.3 kJ mol^{-1}. It is clear that mass transfer is not a reaction's limiting factor, demonstrating that reactions are chemically driven rather than being limited by mass transfer.[53] The plot of the $\ln k$ dependence of $1/T$ shows the acquired data, which supports that it is a first-order reaction.[53]

4. Conclusion

Research on biodiesel transesterification using DESs directly as catalysts and reaction medium are not commonly reported. That is the raison why the catalytic activity of the DESs is reported herein for the first time in this study for the transesterification of microalgae lipid into biodiesel to replace the toxic and corrosive catalyst H_2SO_4. DES ChCl–$SnCl_2$ showed higher catalytic activity in transesterification due to its stronger acidity compared to the DES ChCl–$ZnCl_2$. This was illustrated by geometric optimization of DES structures which showed that the metal centers though furthest from the choline moiety are the most acidic. The FAME conversion of microalgae lipid was 36.75 mg g^{-1} under ideal conditions (molar ratio of methanol to lipid of 6 with 8 vol% DES dosage in methanol at 140 °C for 420 min). Furthermore, the pseudo-first-order reaction mechanism was followed by a kinetic analysis of the reaction wherein the activation energy was 36.3 kJ mol^{-1}, it was evident that mass transfer is not the limiting factor of a reaction, proving that reactions are chemically induced not mass transfer limitation using DES as a catalyst in the transesterification of microalgae lipid to biodiesel. In addition, this study can provide data to contribute to the advancement of an innovative, efficient and environmentally friendly industrial biodiesel production technology. However, more studies are needed to scale up the process before going to commercial application.

Author contributions

ADPN was responsible for performing the experiment, collecting the data, preparing the graphs, and writing the first draft; JX and MAA were responsible for conceptualization the experiment, validation of data, review and editing, supervision, and the obtaining of funding; AZ, WX, SZ, MS were participated in review and editing. The final draft was read by all of the authors, and they all gave their approval.

Conflicts of interest

All the authors declare that "there are no conflicts to declare".

Acknowledgements

The research cost of this fund was received from NSFC (No. 22261132515 and No. 22078308), Innovation Leadership Program in Sciences and Technologies for Central Plains Talent Plan (No. 214200510009), Program for Science & Technology Innovative Research Team in the University of Henan Province (No. 22IRTSTHN007), Innovation Leadership Program in Sciences and Technologies for Zhengzhou Talent Gathering Plan, and Outstanding Contribution Talent Project in Sciences and Technologies for Zhengzhou Talent Gathering Plan (No. 20180400042) and fund from Zhengzhou University.

References

1 H. Qin, X. Hu, J. Wang, H. Cheng, L. Chen and Z. Qi, *Green Energy Environ.*, 2020, **5**, 8–21.
2 S. J. Davis, N. S. Lewis, M. Shaner, S. Aggarwal, D. Arent, I. L. Azevedo, S. M. Benson, T. Bradley, J. Brouwer and Y.-M. Chiang, *Science*, 2018, **360**, eaas9793.

3 C. Zhou, Z. Ge, Y. Wang, F. Shang and L. Guo, *Carbon Neutrality*, 2023, **2**, 1–13.
4 V. Fung, Y. Xiao, Z. J. D. Tan, X. Ma, J. F. J. Zhou, S. Panda, N. Yan and K. Zhou, *Biomaterials*, 2022, **287**, 121661.
5 H. C. Ong, Y. W. Tiong, B. H. H. Goh, Y. Y. Gan, M. Mofijur, I. R. Fattah, C. T. Chong, M. A. Alam, H. V. Lee and A. S. Silitonga, *Energy Convers. Manag.*, 2021, **228**, 113647.
6 A. E.-F. Abomohra, X. Zheng, Q. Wang, J. Huang and R. Ebaid, *Bioresour. Technol.*, 2021, **323**, 124640.
7 R. Singh, A. Kumar and Y. C. Sharma, *Energy Fuels*, 2019, **33**, 1175–1184.
8 C. Cuautli, I. Romero-Ibarra, J. Vazquez-Arenas and M. Galvan, *Fuel*, 2021, **298**, 120840.
9 C. Safi, A. V. Ursu, C. Laroche, B. Zebib, O. Merah, P.-Y. Pontalier and C. Vaca-Garcia, *Algal Res.*, 2014, **3**, 61–65.
10 X. Tan, P. Sudarsanam, J. Tan, A. Wang, H. Zhang, H. Li and S. Yang, *J. Environ. Chem. Eng.*, 2021, **9**, 104719.
11 Y. Liu, H. Yan, J. Liu, W. Dong, Z. Cao, X. Hu and Z. Zhou, *Renewable Energy*, 2020, **162**, 1842–1853.
12 D. Cai, Y. Xie, L. Li, J. Ren, X. Lin and T. Qiu, *Energy Convers. Manag.*, 2018, **166**, 318–327.
13 F. Merza, A. Fawzy, I. AlNashef, S. Al-Zuhair and H. Taher, *Energy Rep.*, 2018, **4**, 77–83.
14 A. P. Abbott, P. M. Cullis, M. J. Gibson, R. C. Harris and E. Raven, *Green Chem.*, 2007, **9**, 868–872.
15 L. Tao, D. Yuefeng, G. Shucai and C. Ji, *Chin. J. Chem. Eng.*, 2010, **18**, 322–327.
16 W. Chen, Y. Liu, L. Song, M. Sommerfeld and Q. Hu, *Algal Res.*, 2020, **52**, 102080.
17 J. Cao, B. Qi, J. Liu, Y. Shang, H. Liu, W. Wang, J. Lv, Z. Chen, H. Zhang and X. Zhou, *RSC Adv.*, 2016, **6**, 21612–21616.
18 D. Liang, J. Wu, L. Lu, R. Fang, J. Xu and M. A. Alam, *Bioresour. Technol.*, 2022, **364**, 128100.
19 F. Jiang, Q. Zhu, D. Ma, X. Liu and X. Han, *J. Mol. Catal. A: Chem.*, 2011, **334**, 8–12.
20 M. J. Frisch, G. W. Trucks, H. B. Schlegel, G. E. Scuseria, M. A. Robb, J. R. Cheeseman, G. Scalmani, V. Barone, B. Mennucci, G. A. Petersson, H. Nakatsuji, M. Caricato, X. Li, H. P. Hratchian, A. F. Izmaylov, J. Bloino, G. Zheng, J. L. Sonnenberg, M. Hada, M. Ehara, K. Toyota, R. Fukuda, J. Hasegawa, M. Ishida, T. Nakajima, Y. Honda, O. Kitao, H. Nakai,T. Vreven, J. A. Montgomery Jr., J. E. Peralta, F. Ogliaro, M. Bearpark, J. J. Heyd, E. Brothers, K. N. Kudin, V. N. Staroverov, R. Kobayashi, J. Normand, K. Raghavachari, A. Rendell, J. C. Burant, S. S. Iyengar, J. Tomasi, M. Cossi, N. Rega, J. M. Millam, M. Klene, J. E. Knox, J. B. Cross, V. Bakken, C. Adamo, J. Jaramillo, R. Gomperts, R. E. Stratmann, O. Yazyev, A. J. Austin, R. Cammi, C. Pomelli, J. W. Ochterski, R. L. Martin, K. Morokuma, V. G. Zakrzewski, G. A. Voth, P. Salvador, J. J. Dannenberg, S. Dapprich, A. D. Daniels, Ö Farkas, J. B. Foresman, J. V. Ortiz, J. Cioslowski, D. J. Fox, Gaussian, Inc., Wallingford CT, 2009.
21 A. D. Becke, *J. Chem. Phys.*, 1992, **96**, 2155–2160.
22 C. Lee, W. Yang and R. G. Parr, *Phys. Rev. B: Condens. Matter Mater. Phys.*, 1988, **37**, 785.
23 P. J. Hay and W. R. Wadt, *J. Chem. Phys.*, 1985, **82**, 299–310.
24 A. D. P. Ngatcha, G. Muhammad, Y. Lv, W. Xiong, A. Zhao, J. Xu and M. A. Alam, *Biomass Convers. Biorefin.*, 2022, **12**, 133–143.
25 W. Lu, M. A. Alam, Y. Pan, W. J. Nock, Z. Wang and Z. Yuan, *Korean J. Chem. Eng.*, 2016, **33**, 2575–2581.
26 S. A. Trujillo, D. Peña-Solórzano, O. R. Bejarano and C. Ochoa-Puentes, *RSC Adv.*, 2020, **10**, 40552–40561.
27 S. Abdulkadir and M. Tsuchiya, *J. Exp. Mar. Biol. Ecol.*, 2008, **354**, 1–8.
28 S. Sadaf, J. Iqbal, I. Ullah, H. N. Bhatti, S. Nouren, J. Nisar and M. Iqbal, *Sustain. Cities Soc.*, 2018, **41**, 220–226.
29 Q. Fanglong, S. Jinhe, X. Shaolei, S. Chenglong and J. Yongzhong, *Int. Proc. Chem., Biol. Environ. Eng.*, 2015, **90**, 70–75.
30 Y.-l. Yang and Y. Kou, *Chem. Commun.*, 2004, 226–227.
31 M. Moggio, S. Errico, N. Diano and M. Lepore, *Eng. Proc.*, 2021, **10**, 9.
32 V. Shapaval, J. Brandenburg, J. Blomqvist, V. Tafintseva, V. Passoth, M. Sandgren and A. Kohler, *Biotechnol. Biofuels*, 2019, **12**, 1–12.
33 A. C. M. Loy, A. T. Quitain, M. K. Lam, S. Yusup, M. Sasaki and T. Kida, *Energy Convers. Manage.*, 2019, **180**, 1013–1025.
34 M. R. Nizah, Y. Taufiq-Yap, U. Rashid, S. H. Teo, Z. S. Nur and A. Islam, *Energy Convers. Manage.*, 2014, **88**, 1257–1262.
35 G. Muhammad, A. D. P. Ngatcha, Y. Lv, W. Xiong, Y. A. El-Badry, E. Asmatulu, J. Xu and M. A. Alam, *Renewable Energy*, 2022, **184**, 753–764.
36 N. Duongbia, S. Chaiwongsar, C. Chaichana and S. Chaiklangmuang, *Biomass Convers. Biorefin.*, 2019, **9**, 305–319.
37 A. Rezayan and M. Taghizadeh, *Process Saf. Environ. Prot.*, 2018, **117**, 711–721.
38 X. Han, W. Yan, C.-T. Hung, Y. He, P.-H. Wu, L.-L. Liu, S.-J. Huang and S.-B. Liu, *Korean J. Chem. Eng.*, 2016, **33**, 2063–2072.
39 H. Pan, H. Li, X.-F. Liu, H. Zhang, K.-L. Yang, S. Huang and S. Yang, *Fuel Process. Technol.*, 2016, **150**, 50–57.
40 S. Ghosh, S. Banerjee and D. Das, *Algal Res.*, 2017, **27**, 12–20.
41 J. Cheng, Y. Qiu, R. Huang, W. Yang, J. Zhou and K. Cen, *Bioresour. Technol.*, 2016, **221**, 344–349.
42 M. Yadav, V. Singh and Y. C. Sharma, *Energy Convers. Manage.*, 2017, **148**, 1438–1452.
43 H. Zhang, H. Li, H. Pan, X. Liu, K. Yang, S. Huang and S. Yang, *Energy Convers. Manag.*, 2017, **138**, 45–53.
44 M. Khalekuzzaman, S. B. Kabir, M. Islam, P. Datta, M. Alam and J. Xu, *Biomass Convers. Biorefin.*, 2021, **11**, 767–779.
45 G. Knothe, *Energy Fuels*, 2008, **22**, 1358–1364.
46 K. Bajwa, N. R. Bishnoi, A. Kirrolia, S. Gupta and S. T. Selvan, *Appl. Water Sci.*, 2019, **9**, 1–16.
47 A. Kirrolia, N. R. Bishnoi and R. Singh, *Ann. Microbiol.*, 2014, **64**, 1133–1147.

48 J. K. Suastes-Rivas, R. Hernández-Altamirano, V. Y. Mena-Cervantes, E. J. B. Gómez and I. Chairez, *Fuel*, 2020, **280**, 118633.
49 V. K. Booramurthy, R. Kasimani, D. Subramanian and S. Pandian, *Fuel*, 2020, **260**, 116373.
50 N. Kaur and A. Ali, *RSC Adv.*, 2014, **4**, 43671–43681.
51 I. Lukić, Ž. Kesić, S. Maksimović, M. Zdujić, H. Liu, J. Krstić and D. Skala, *Fuel*, 2013, **113**, 367–378.
52 N. Kaur and A. Ali, *Renewable Energy*, 2015, **81**, 421–431.
53 N. Kaur and A. Ali, *Appl. Catal., A*, 2015, **489**, 193–202.